# NONLINEAR INTERACTIONS OF $CO_2$ LASER RADIATION WITH PLASMAS

F. F. Chen and C. Joshi

PPG-803

July, 1984

CENTER FOR
PLASMA PHYSICS
AND
FUSION ENGINEERING

UNIVERSITY OF CALIFORNIA
LOS ANGELES

# NONLINEAR INTERACTIONS OF $CO_2$ LASER RADIATION WITH PLASMAS

F. F. Chen and C. Joshi

PPG-803

July, 1984

This is the final technical report, minus appendices, for National Science Foundation Grant ECS 80-03558, Aug. 1, 1980-Jan. 31, 1984.

Electrical Engineering Department
School of Engineering and Applied Science
University of California, Los Angeles

FINAL TECHNICAL REPORT

NATIONAL SCIENCE FOUNDATION

Division of Electrical, Computer, and Systems Engineering

Quantum Electronics, Waves, and Beams Program

Grant No. ECS 80-03558

for

# NONLINEAR INTERACTIONS OF $CO_2$ LASER RADIATION WITH PLASMAS


Principal Investigator: Francis F. Chen
Professor of Electrical Engineering

Co-principal Investigator: Chan Joshi
Adjunct Associate Professor


Period covered: August 1, 1980 - January 31, 1984


Electrical Engineering Department

School of Engineering and Applied Science

University of California, Los Angeles

Los Angeles, California 90024

TABLE OF CONTENTS

## I. SUMMARY OF RESULTS

The proposed task for this grant period was the systematic investigation of the nonlinear and parametric interactions of intense electromagnetic radiation with matter in the plasma state. Our guiding philosophy was to isolate the different phenomena by careful design of the experiments--particularly the plasma targets--so that one effect could be studied at a time. The program has succeeded well; and we can claim to have 1) made the first direct observation of filamentation, 2) discovered the phenomenon of resonant self-focusing, 3) solved the mystery of the low saturation level of stimulated Brillouin scattering observed at low intensities, 4) made the first clean observation of stimulated Raman scattering in a system free from Brillouin scatter, and 5) excited plasma waves by $CO_2$ optical mixing for the first time, with direct detection of the waves by Thomson scattering.

The achievement of these results is due in large part to the painstaking development of two experimental systems: a ruby-laser Thomson scattering apparatus with space and time resolution; and a well-characterized, stable, and uniform theta pinch plasma target. The workhorse 40-J $CO_2$ laser chain, arc plasma source, and He-cooled detectors were already available; but the two new systems were perfected during this grant period.

The main results are summarized here; references are to the publications listed in Sec. II.

1. Filamentation. By using a Fourier-optics technique, we have produced photographs of plasma striations produced by the filamentation instability (Ref. 1).

2. Resonant self-focusing. Optical mixing of co-propagating 9.6 and 10.3 μm beams is found to produce anomalous refraction of the beams without frequency shift. This is explained theoretically by the resonant

excitation of plasma waves, which subsequently blow out a density channel by their ponderomotive force. The presence of the plasma waves is confirmed by observing a red-shifted line at 11.0 μm. (Ref. 3, Appendix 1).

3. Stimulated Brillouin scattering. This dangerous instability, first predicted and observed at UCLA, has been under study here for many years. Though the threshold was verified to agree with theory, the saturation level of $\leq$10% has been a mystery (Ref. 4). To solve this, space- and time-resolved measurements of the ion wave amplitude were made by Thomson scattering (Refs. 6, 17; Appendix 2). This work was Chris Clayton's thesis. Harmonic generation was found not to be the cause, contrary to theoretical predictions. Instead, the data can be fit only by a theory of ion trapping (Refs. 15, 17; Appendix 3). Our understanding of this instability is now perhaps 80% complete.

4. Stimulated Raman scattering. Though we were not the first to observe SRS in an underdense plasma unencumbered by critical and quarter-critical layer phenomena, previous experiments were complicated by the coexistense of SBS, which usually has a lower threshold. To avoid this, student B. Amini built a theta-pinch with $T_i \geq T_e$, so that ion waves suffer heavy Landau damping and SBS cannot occur. Clean pulses of SRS near theshold are seen (Ref. 19). The theta-pinch target is fully ionized, uniform, and quiescent, as confirmed by simultaneous dual-axis interferometry (Sec. III); and no SBS is detectable above $10^{-6}$ of the SRS level (Ref. 34). The SRS threshold is about an order of magnitude below theory (Ref. 16; Appendix 4), but the same discrepancy is seen by others (Ref. 24). The mystery is not yet solved.

5. Beat-frequency excitation. Numerous theorists have predicted the strong coupling of laser light to plasma waves, and the uses thereof,

when opposing beams have a difference frequency equal to $\omega_p$. Until now, the difficulty of having two stable beams overlapping in space and time and of detecting the plasma wave have prevented four groups from achieving this result with $CO_2$ lasers. As the major part of his dissertation, B. Amini has now done this with Thomson scattering detection (Refs. 20, 33, 34; Appendix 6). The result is exceptionally clean because the plasma wave satellites are seen in Thomson scattering, so that the plasma density is absolutely calibrated.

6. Rayleigh-Taylor instability. As a by-product of calibrating the plasma source, B. Amini has elucidated the stable and unstable regimes of the theta-pinch (Ref. 18; Sec. III of this report).

7. Stark satellites. In measuring the plasma temperature and density spectroscopically, Amini found satellites in the Stark profile of He II 4686 Å which appear to be harmonics of a plasma instability frequency. Though excitation of forbidden satellites by electric fields (anomalous Stark effect) has been seen before, this is the first time it has been seen on an allowed line of a hydrogen-like atom. This may be a useful new technique in the study of laser-plasma interactions (Ref. 26).

8. SRS in a rippled plasma. H. C. Barr and F. F. Chen have considered the effect on SRS of a density ripple caused by SBS. The main effect is mode-coupling to modes with higher and lower k, including k=0. Two new frequencies arise, one higher and one lower than the uniform-plasma mode. The latter suffers a reduced growth rate, but the ripple causes the new modes to grow. A surprising result is that one of the new modes has a backward-moving component larger than that which is excited. This is explained physically, with implications for acceleration of electrons. (Refs. 19, 25).

9. Laser-plasma interactions at 0.35 μm. Work done at the National Laser Users' Facility at Rochester has given information on parametric instabilities at shorter wavelengths and higher densities (Refs. 13, 14, 21, 22, 31, 32).

10. Laser-driven accelerators. Our work on beat-excitation has led naturally to our next major research effort, testing the possibility of GeV or TeV accelerators driven by lasers. The beat-wave accelerator and surfatron concepts invented at UCLA and preliminary results are described in Refs. 7-12, 23, 28, and 30.

11. One-shot x-ray spectra. Work with JPL has produced a new x-ray diagnostic which can give a one-shot spectrum without a dispersive element (Ref. 27).

II. RELEVANT PUBLICATIONS, 8/1/80 - 1/31/84


1. C. Joshi, C. E. Clayton, A. Yasuda, and F. F. Chen, "Direct Observation of Laser Beam Filamentation," J. Appl. Phys. 53, 215 (1982).

2. C. E. Clayton, C. Joshi, A. Yasuda, and F. F. Chen, "Dependence of Stimulated Brillouin Scattering on Target Material and f-number," Phys. Fluids 24, 2312 (1981).

3. C. Joshi, C. E. Clayton, and F. F. Chen, "Resonant Self-focusing of Laser Light in a Plasma," Phys. Rev. Letters 48, 874 (1982).

4. F. F. Chen, C. Joshi, C. E. Clayton, B. Amini, and H. C. Barr, "Experiments on Nonlinear Phenomena in Underdense Plasmas," Proc. U.S.-Japan Seminar on Theory and Application of Multiply Ionized Plasmas Produced by Laser and Particle Beams, Nara, Japan, 1982, pp. 243-255.

5. C. E. Clayton, H. Huey, C. Pawley, A. Y. Lee, B. Amini, F. F. Chen, C. Joshi, and N. C. Luhmann, Jr., "Experimental Modeling of Laser-Plasma Interaction Physics," Proc. 9th Int'l Conf. on Plasma Physics and Controlled Nuclear Fusion Research, Baltimore, Maryland, 1982 (IAEA, Vienna), Vol. I, pp. 105-113.

6. C. E. Clayton, C. Joshi, and F. F. Chen, "Space and Time Evolution of SBS Ion Wave Harmonics," in Laser Interaction and Related Plasma Phenomena, ed. by H. Hora and G. Miley, Vol. 6, pp. 621-631 (Plenum, 1984).

7. C. Joshi, T. Tajima, and J. M. Dawson, "Forward Raman Instability and Electron Acceleration," Phys. Rev. Letters 47, 1285 (1981).

8. C. Joshi, "The Plasma Beat Wave Accelerator I: Experiments," Proc. of the Workshop on the Laser Acceleration of Particles, in Laser Acceleration of Particles, ed. by P. J. Channell, American Institute of Physics Conf. Proc. Series, No. 91, pp. 28-42.

9. C. Joshi, "The Plasma Beat Wave Accelerator," Proceedings of the ECFA-RAL Meeting, Oxford, United Kingdom, 1982, pp. 195-208.

10. C. Joshi, "The Surfatron Laser-Plasma Accelerator: Prospects Limitations," Workshop on Laser and Plasma Collective Accelerators, International Centre for Theoretical Physics, Trieste, Italy, 1983.

11. T. Katsouleas, J. M. Dawson, W. Mori, and C. Joshi, "A Plasma Wave Accelerator--Surfatron I and II," UCLA PPG-690 (1983).

12. T. Katsouleas, C. Joshi, W. Mori, and J. M. Dawson, "Prospects of the Surfatron Laser Plasma Accelerator," Proc. of 12th International Conf. on High-Energy Physics, Fermi National Accelerator Laboratory, August 11-16, 1983, pp. 460-462.

13. H. Figueroa, C. Joshi, C. E. Clayton, H. Azechi, N. A. Ebrahim, and K. Estabrook, "High Frequency Instabilities in Underdense Plasmas Produced by a 0.35 μm Laser Beam," in Laser Interaction and Related Plasma Phenomena, Vol. 6, pp. 527-543, (Plenum, 1984).

14. H. Azechi, N. A. Ebrahim, H. Figueroa, and C. Joshi, "Hot Electron Generation in UV Laser Irradiated Underdense Plasmas," Proc. 9th Int'l Conf. on Plasma Physics and Controlled Nuclear Fusion Research, Baltimore, Maryland, 1982 (IAEA, Vienna), Vol. I, pp. 115-123.

15. C. E. Clayton, C. Joshi, and F. F. Chen, "Ion Trapping Saturation of the Brillouin Instability," Phys. Rev. Letters 51, 1656 (1983).

16. B. Amini and F. F. Chen, "Collisional and Convective Thresholds for Raman Backscatter," UCLA PPG-746 (1983).

17. C. Clayton, Thesis, UCLA PPG-759 (1983).

18. B. Amini, "Evolution of the Rayleigh-Taylor Instability Driven by ∇B," UCLA PPG-780 (1984).

PAPERS PUBLISHED SINCE 1/31/84 OR IN PREPARATION

19. F. F. Chen, B. Amini, C. E. Clayton, and H. C. Barr, "Excitation of Ion and Plasma Waves by Laser Beams," Proc. Int'l Conf. on Plasma Physics, Lausanne, 1984, pp. 271-272.

20. B. Amini and F. F. Chen, "Thomson-scattering Detection of Plasma Waves Excited by Two Laser Beams," submitted to Phys. Rev. Letters (1984).

21. H. Figueroa, C. Joshi, H. Azechi, N. A. Ebrahim, and K. Estabrook, "Stimulated Scattering and Hot Electron Generation in Underdense Plasmas Produced by a 0.35 μm Laser Beam," accepted by Physics of Fluids (1984).

22. H. Azechi, N. A. Ebrahim, H. Figueroa, and C. Joshi, "Laser Induced Density Fluctuations and the Two-Plasmon Decay Instability at 0.35 μm," submitted to Phys. Rev. Letters (1984).

23. C. Joshi, W. Mori, T. Katsouleas, J. M. Dawson, J. M. Kindel, and D. W. Forslund, "Ultra-high Gradient Particle Acceleration by Intense Laser-Driven Plasma Density Waves," accepted by Nature (1984).

24. F. F. Chen, "The Convective Raman Threshold in Blue Light," UCLA PPG-791 (1984).

25. H. C. Barr and F. F. Chen, "Stimulated Raman Scattering in a Rippled Plasma," Phys. Fluids (1984, in preparation).

26. B. Amini and F. F. Chen, "Detection of High Frequency Instability Through the Satellites of a He II Line," Anomalous Absorption Conference, Charlottesville, Va., 1984 (abstract; paper in preparation).

27. K. Marsh, C. Joshi, J. R. Janesick, and S. A. Collins, "Nondispersive X-ray Spectroscopy and Imaging of Plasmas Using a Charged Coupled Device," Bull. Amer. Phys. Soc. (1984).

28. C. Darrow, C. E. Clayton, D. Umstadter, and C. Joshi, "Experimental Studies of Wave-Particle Interaction," Bull. Amer. Phys. Soc. (1984).

29. W. Mori, C. Joshi, J. M. Dawson, J. M. Kindel, and D. W. Forslund, "Computer Simulations of Two-Plasmon Decay," Bull. Amer. Phys. Soc. (1984).

30. T. Katsouleas, F. F. Chen, C. E. Clayton, J. M. Dawson, C. Joshi, and W. Mori, "Studies of the Plasma Beat Wave Accelerator," Bull. Amer. Phys. Soc. (1984).

31. C. Joshi, H. Figueroa, and C. E. Clayton, "Observation of Forward Scattering and Filamentation at 0.35 μm," Bull. Amer. Phys. Soc. (1984).

32. H. Figueroa, C. Joshi, and C. E. Clayton, "Studies of Stimulated Raman Backscattering from Long, Underdense Plasmas," Bull. Amer. Phys. Soc. (1984).

33. B. Amini, "Absolute Amplitude of Electron Plasma Wave Excited by Two Laser Beams," Bull. Amer. Phys. Soc. (1984).

34. B. Amini, Thesis, UCLA (1984), in preparation.

35. B. Amini and F. F. Chen, "The Convective Raman Instability," (in preparation).

III. SCIENTIFIC DETAILS

A. Stimulated Brillouin Scattering

Our previous work on SBS[1-7,9] (numbers refer to the publications listed in Sec. V) has confirmed many features of the linear theory of this parametric instability: the convective threshold, polarization, sidescatter, z-dependence, bandwidth dependence, etc. On the other hand the spiky nature of the scattered signal and the low saturation level remained unexplained. During the past year, we have probed the ion wave generated in SBS in an effort to understand the details of the interaction. The discrepancy of the saturation level with theory is shown in Figs. 1 and 2.

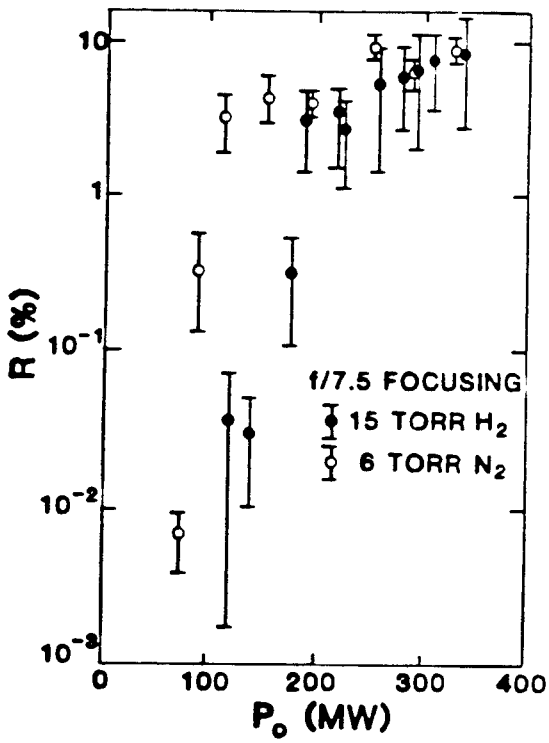


Fig. 1

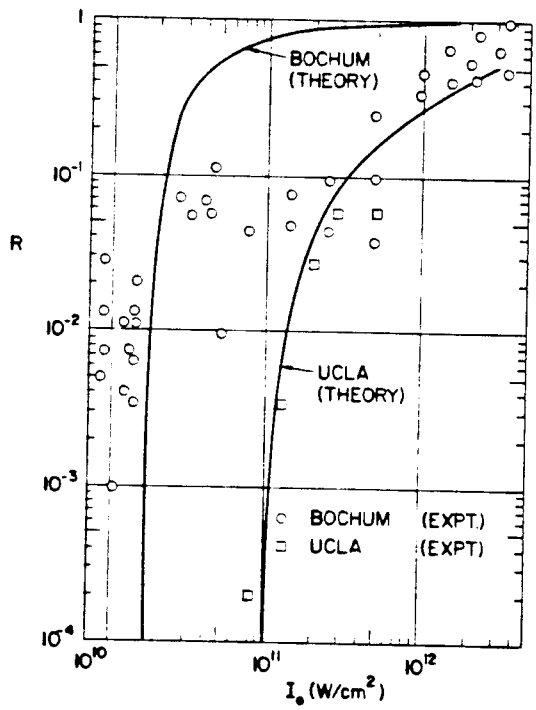


Fig. 2

In Fig. 1 we show typical data on SBS reflectivity as a function of input laser power. It is seen that saturation is reached at about 8%. The saturation mechanism that seems to explain observations made with large lasers is ion heating: the ion acoustic wave heats ions, increasing $T_i/T_e$ and therefore increasing Landau damping so that further growth of the ion wave is slowed down. We have computed the ion heating limit for long, slender interaction regions, where radial heat conductivity determines the temperature, and these curves are shown in Fig. 2 for our experiment and a similar one done at high intensities in Bochum, Germany. It is seen that the UCLA points (squares) fit the theory well at low intensities but level off well below the ion heating limit. The Bochum points (circles) also fall below the theoretical curve, though large reflectivities of order unity can ultimately be obtained by increasing the intensity to above $10^{12}$ W/cm$^2$.

These experiments were done with the apparatus shown in Fig. 3, consisting of a 40-J, 40-ns $CO_2$ laser; an arc preionized plasma target of

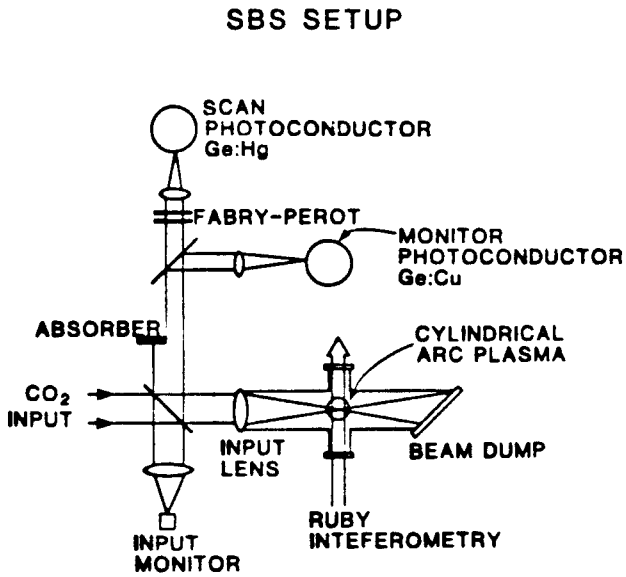


Fig. 3

density $\approx 2\times10^{17}$ $cm^{-3}$; liquid He cooled photoconductor detectors; a ruby laser for Thomson scattering; and a ruby light detection system comprising a two-meter spectrograph, an optical multichannel analyzer, and a streak camera borrowed from Livermore. Since backscatter in underdense plasmas ($n/n_c \approx 0.02$ in our case) requires $k \approx 2k_o$, the wave number of the excited ion wave is fixed by the $CO_2$ pump. Since the ruby light has another k which is fixed, the k-matching condition for Thomson scattering requires the scattering angle to be $7.5^o$. The set-up for this is shown in Fig. 4.

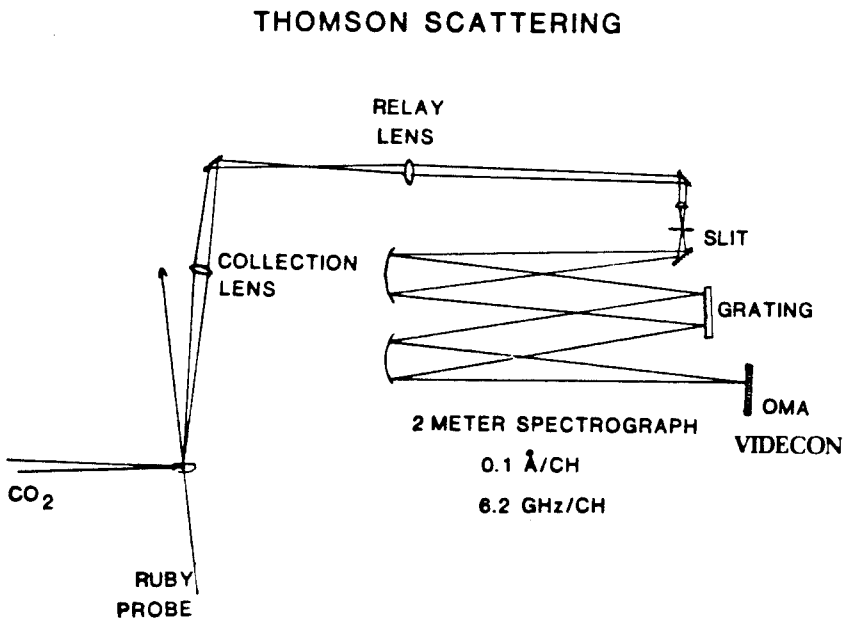


Fig. 4

Time-integrated ruby scattering indeed shows that the light is sharply collimated at $7.5^o$, and that the frequency shift corresponds to the ion wave frequency as measured from the $CO_2$ backscatter. Axial and radial scans gave the expected spatial extent of the ion wave; these measurements are shown in Ref. 11. The ion wave is seen to grow exponentially in the

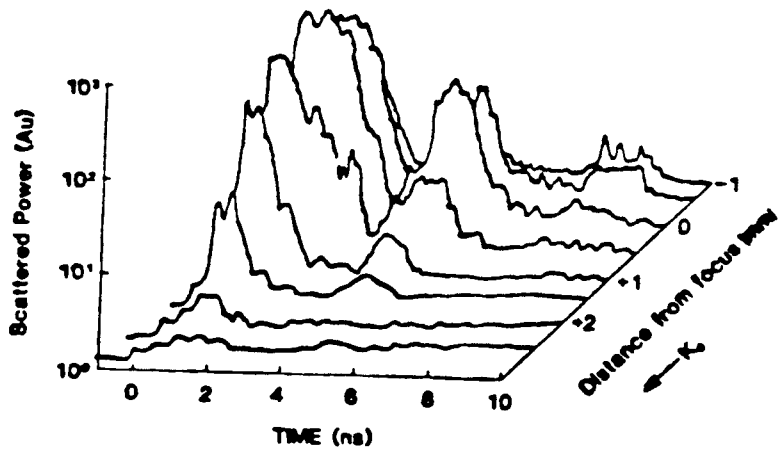


Fig. 5

direction. Why the coherence time of the ion wave is so short is not yet understood, but these measurements show, at least, that the spikiness of the backscatter is due to the ion wave itself, not to an interference between ion waves in different regions of the plasma.

To see whether or not harmonic generation could explain the saturation level, we modified the vacuum chamber to allow Thomson scattering to be measured at $2\times7.5^{\circ}$ and $3\times7.5^{\circ}$, giving the 2k and 3k spatial harmonics of the ion wave. The results (Fig. 6) show very large harmonics ($\approx$10% of the fundamental) but nothing in between. These harmonics, however, do not account for saturation, because their amplitudes scale linearly with the fundamental, not with the square.

The question then arises: Are these harmonics (also seen by the group at NRC, Ottawa) real, or are they artifacts of the Thomson scattering method? Chris Clayton gave this question considerable thought and calculation; his conclusions follow.

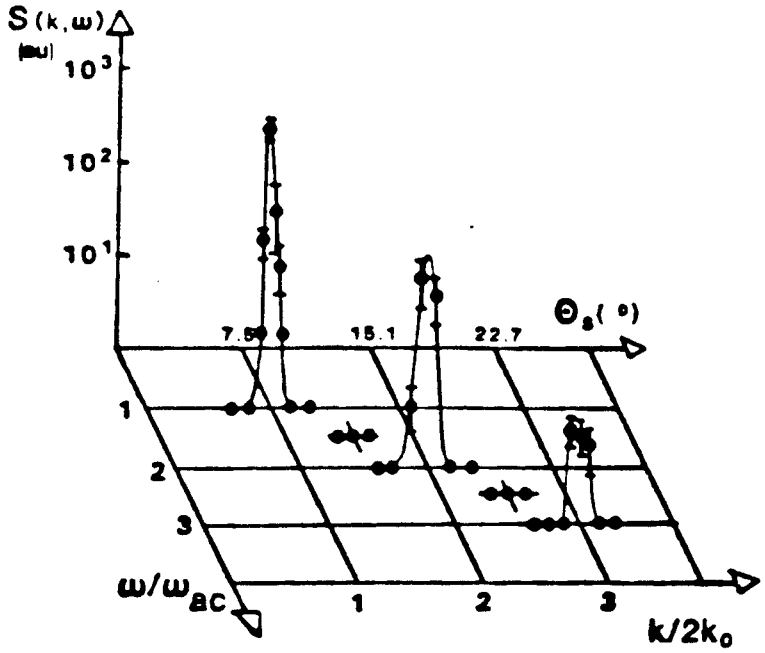


Fig. 6

There are several mechanisms which could conceivably give rise to harmonics in the collective Thomson scattered light. For example, even if the ion wave were a pure sinusoid, higher order (larger angle) diffraction can occur through the Raman-Nath or phase grating diffraction effect. To analyze this possibility, we treat the ion wave as a refractive medium (neglect scattering) and solve for the angular distribution of the probe beam after traversing a sinusoidally varying and traveling medium. We find that this does produce "harmonics" in that each order n is frequency shifted by $n\omega_{ac}$. However, the power in the second order to that in the first order should be less than $10^{-5}$. Experimentally, we find a ratio more like $10^{-1}$. Therefore, the phase grating effect is not causing our observed harmonics. More evidence against the phase grating effect is that we find the scattered power in the harmonics to be a strong

function of k-mismatch, whereas k-matching is not very important for a phase grating.

Another possible "fluke" is that the $CO_2$ pump beam itself is spatially phase modulated by the ion acoustic wave. This causes the pump beam to have spatial harmonics at multiples of $k_o$, e.g., at $3k_o$. The $3k_o$ spatial harmonic of the pump beam can interact with the $1k_o$ SBS backscattered beam to modulate the plasma at $4k_o$, thus conceivably exciting the second harmonic of the ion acoustic wave. However this, too, is a negligeable effect.

> AUTHOR'S NOTE: It's a bit more involved than this. The trouble with the above description is that the beat frequency is just $\omega_{ac}$. Thus, it wouldn't be a resonant excitation. Thus the word "conceivable".

Collective Thomson scattering is often referred to as Bragg scattering. Indeed, Bragg scattering of X-rays from the periodic electron distributions in crystals is very much like collective Thomson scattering from the periodic electron distributions in an ion wave. The analogy has its limits, however. In Bragg scattering, one can arrange to scatter in first, second, or higher order according to the Bragg condition

$$\sin \theta = n\lambda/2d.$$

The question this poses is: Can one do "second order" Thomson scattering from a purely sinusoidal ion wave?

To answer this question, we have carried out the Thomson scattering calculation in an analogous manner to the usual Bragg scattering calculation. The result is that the power scattered into higher orders is proportional to the Fourier coefficients of the electron spatial distribution in the ion acoustic wave. In other words, a purely sinusoidal ion wave cannot be observed in second order. The ion wave itself must be

distorted (i.e., have harmonic content) in order to observe higher order scattering. We conclude, then, that our observed second and third harmonics are indicative of a distorted ion wave.

The large amplitudes of the harmonics remains an intriguing, baffling mystery.

## B. Stimulated Raman Scattering

### 1. Introduction

Though our experiment on SRS was started many years ago, we have only recently observed the phenomenon in an unambiguous way. The main problem has been source development--the creation of a theta-pinch plasma with reproducible density and sufficient uniformity. Meanwhile, two competing groups have published their observations of SRS. The first group--at the University of Washington--originally used a theta-pinch target, but they saw SRS at intensities below the convective threshold. Subsequently, they have made more believable measurements in a colliding shock, but the plasma is so short lived that its parameters and quiescence level cannot be accurately determined. The second group--at the University of Alberta--has made detailed measurements of SRS in a laser-created plasma whose density profile was not reported. The SRS was seen not at the peak of the pulse, but only during after-pulses in the tail. These after-pulses were attributed to feedback into the laser amplifier from Brillouin backscatter. Thus, SRS was always complicated by SBS. In our experiment, the $T_e \simeq T_i$ condition in a $\theta$-pinch suppresses SBS, and indeed we are able to see SRS at the peak of the laser pulse without any observable SBS. Furthermore, we have succeeded in starting SRS from a finite level by sending a red-shifted beam backward through the plasma and optically mixing it with the main beam. Completion of this work will become the main part of B. Amini's thesis. His progress report follows.

### 2. Source development and diagnosis

The theta-pinch device in which the experiments are conducted has a 22.5 cm long copper coil with a 10 cm i.d. and a 2.5 cm gap at the

middle. The quartz discharge tube has a 7.5 cm i.d. with three mid-plane ports $90^{o}$ apart in azimuth. Each port has a 2 cm clear aperture to provide access for optical and internal plasma diagnostics.

By using a parallel plate transmission line, the inductance of the system is minimized and is mainly the inductance of the coil, thus giving a fast pinch (4.3 μsec period). This is about twice as fast as an average pinch. To better understand the field pattern, especially at the ends of the coil, a computer program was developed to plot the lines of force and $B^2(r, z)$. A sample plot is shown in Fig. 7, in which the coil was approximated by 82 current hoops. This was a dc calculation which did not account for the conducting boundary condition for pulses shorter than the skin time. Actually, the field is more uniform than shown, but the difference is slight because only the very outermost field lines cross the coil anyway.

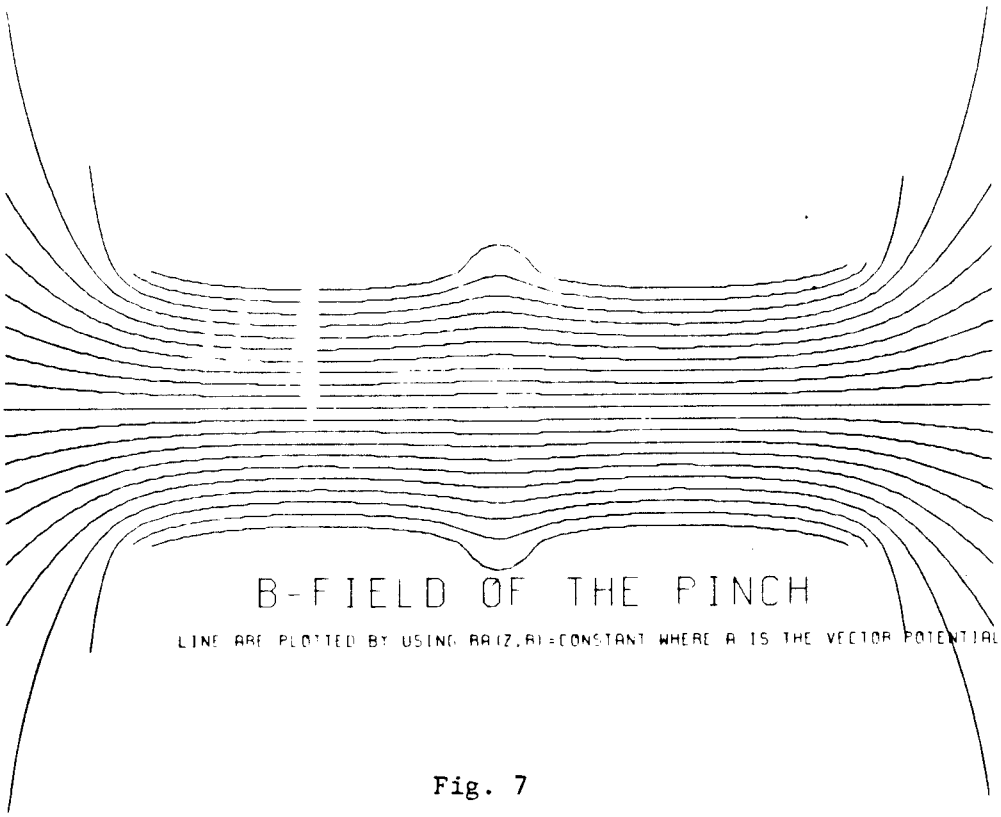


Fig. 7

For the two experiments which will be described later the operating parameters are:

Electron density for Raman scattering = $8 \times 10^{16}$ $cm^{-3}$

Electron density for optical mixing = $6 \times 10^{16}$ $cm^{-3}$

Bank voltage = 28.5 kV

Maximum current = 460 kA

Maximum B-field = 24 kG

Energy storage = 4.5 kJ, 11.1 μF

The operating voltage is capable of being increased up to 40%. Plasma density is a function of filling pressure and operating voltage, and the measured density ranges from $3 \times 10^{16}$ to $9 \times 10^{17}$ $cm^{-3}$. A pick-up loop (diamagnetic loop) mounted around the chamber away from the copper coil measures a fraction of the total flux through the coil and the changes in flux due to currents in the plasma. Plasma radiation at the center of the chamber is collected by a small lens and imaged on a photodiode. Fig. 8a shows a typical trace of the loop signal (1 μsec/cm) whose amplitude is proportional to B or the azimuthal E-field. Fig. 8b is a typical trace of the photodiode signal on a 500 nsec/cm scale. The first peak

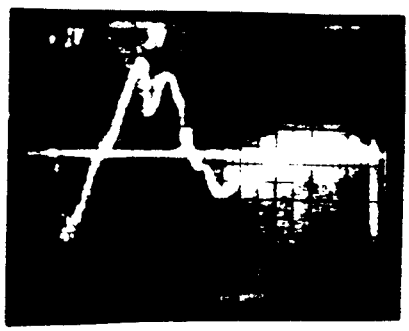

Fig. 8a

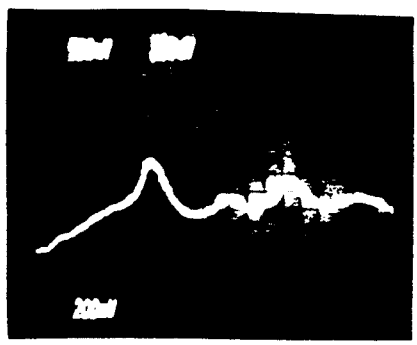

Fig. 8b

of the photodiode corresponds to the maximum compression at 2.3 cm on Fig. 8b, and to the local maximum at 4 cm on Fig. 8a.

Since the electric field is maximum just inside the chamber, the gas breaks down here (at around 3.5 divisions in Fig. 8a) and produces a conducting plasma. We use no preionization, and the trapped field is essentially zero. The increasing magnetic field pushes the plasma sheath inwards until $B^2/8\pi$ equals nKT. This point of maximum compression occurs at about 600 nsec, as seen in Fig. 8a. (This time varies for different gases.) We shall use the 600 nsec figure later in estimating $T_i$. Maximum compression does not coincide with maximum magnetic field. At maximum field (4.5 divisions in Fig. 8a and 5.5 divisions on Fig. 8b), the plasma is somewhat warmer and less dense.

The density is measured by holographic interferometry. Fig. 9 shows the set-up for simultaneous end-on and side-on double exposure holography with a 25-nsec ruby pulse. To show the plasma shape more

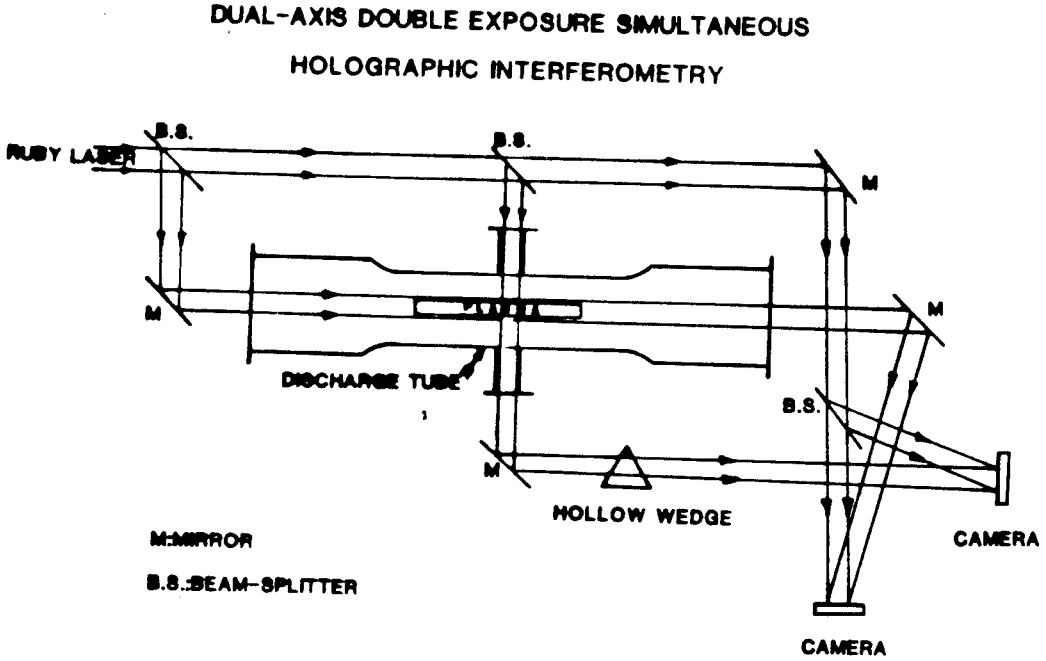


Fig. 9

clearly, the hollow wedge is removed for the end-on interferograms, so that there are no background fringes; for the side-on views, the spacing of the fringes can be arbitrarily adjusted. The end-on views integrate over irrelevant parts of the plasma near the coil ends, but no Abel inversion is needed. The side-on views measure the density at exactly the place where SRS occurs, but Abel inversion is required. The absolute density can be determined accurately by using the profile from the end-on view to invert the side-on views.

The side-on pictures also give directly the axial scalelength $L_n$ which determines the convective Raman threshold. (Note that $L_n$ is different from the interaction length L, which is related to the focal depth of the pump beam.) To obtain $L_n$, we fit the fringe shifts at x = 0 and x = ±1 cm, visible through the 2-cm clear aperture of the side port (a distance of 2000 $\lambda_o$) to a parabolic profile $n = n_o(1 - x^2/L_n^2)$. We find $L_n \geq 15$ cm.

Figs. 10-18 show some of the interferometer data. Fig. 10 contains the timing pulses from five shots, showing the reproducibility. The traces are photodiode signals of plasma light on axis; the ruby laser pulse can be seen superimposed on the first maximum, when the highest density is achieved. The plasma oscillates in radius serveral times during each compression of the magnetic field. The photodiode signal has been calibrated by interferometry and serves as a rough but easy indicator of plasma density.

Figs. 11-13 are end-on interferograms at 75 microns of He, spaced 100 ns apart around the time of peak light. These patterns are reproducible. Each fringe corresponds to $n = 1.25 \times 10^{16}$ cm$^{-3}$. The ruby beam is ≈ 3 cm in diameter, so these pictures show only the compressed

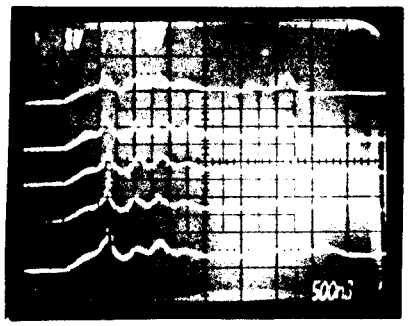

Fig. 10

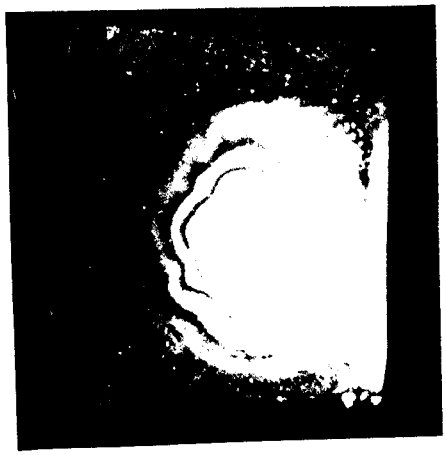


Fig. 11


Fig. 12


Fig. 13

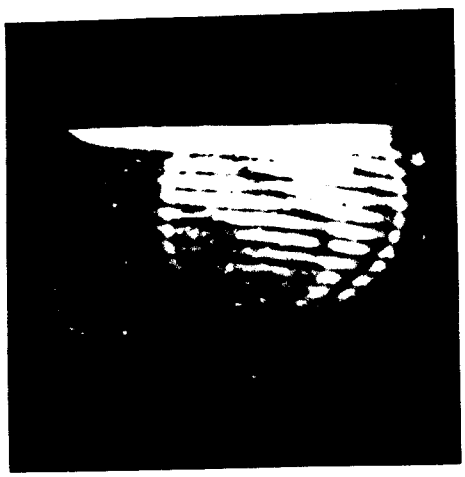


Fig. 14

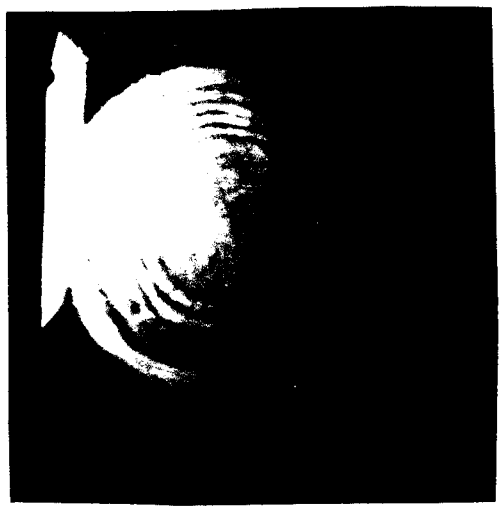


Fig. 15

Fig. 16

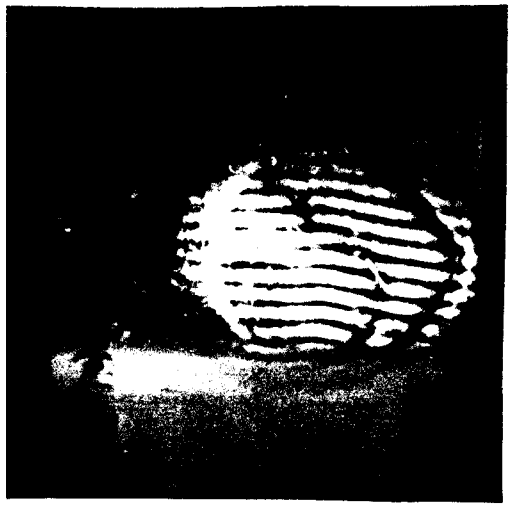

Fig. 17

Fig. 18

plasma at the center of the 7.6-cm diameter chamber. The absence of fringes at the center of the patterns shows that the density is uniform over a 6-mm diameter on axis. Fig. 14 is a side-on interferogram under the same conditions as in Fig. 13; together, these show that $n = 6 \times 10^{16}$ $cm^{-3}$. Figs. 15 and 16 are end-on views at 85 microns pressure at t = -100 and 0 ns. Fig. 17 is side-on view corresponding to Fig. 16. Fig. 18 shows the flute instability occurring at higher voltage and higher pressure (150 microns); the onset of instability is reproducible.

Figs. 19 and 20 show computer analysis of the interferograms of Figs. 13 and 14. Fig. 19 is a radial density profile generated from the central fringe in Fig. 14 by fitting the fringe shift profile to a ninth degree polynomial and then Abel inverting it. This gives a central density of $5 \times 10^{16}$ $cm^{-3}$, but this figure is not very accurate because of the small shifts involved and because of distortions in the beam splitter. Fig. 20 is a radial fringe shift profile generated from the end-on interferogram of Fig. 13, where the density profile is easier to measure.

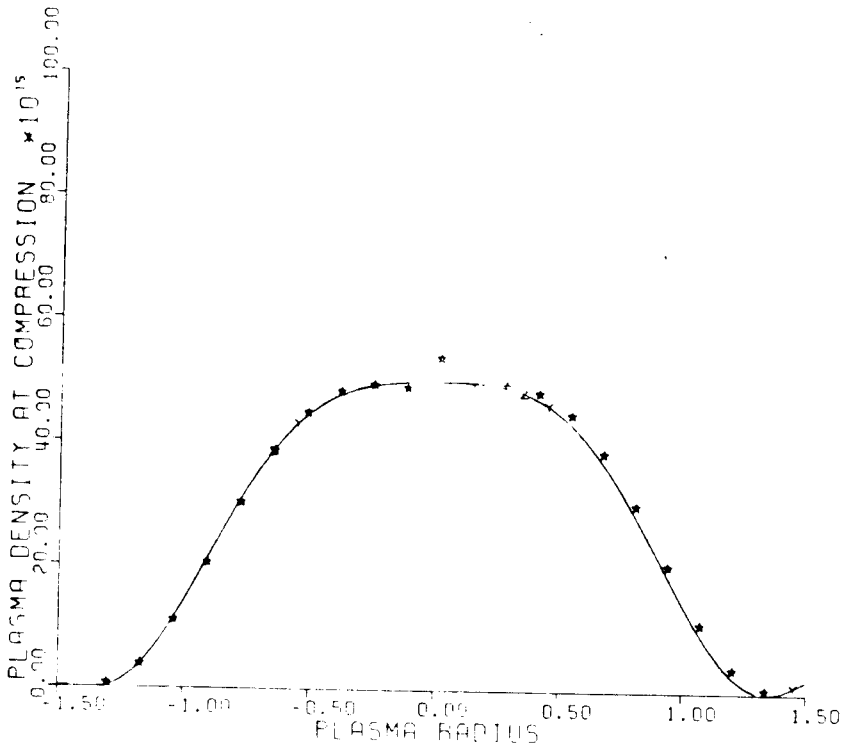


Fig. 19

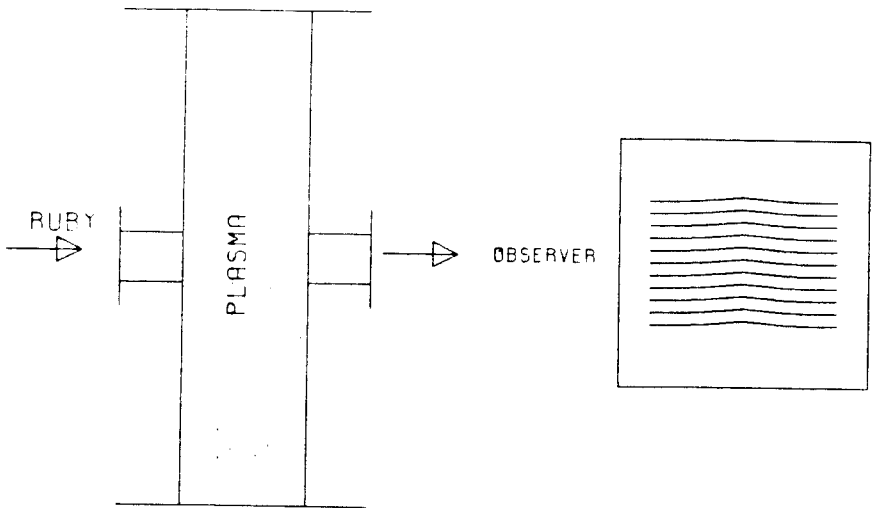


ABEL INVERSION OF AXIAL INTERFEROGRAM

Fig. 20

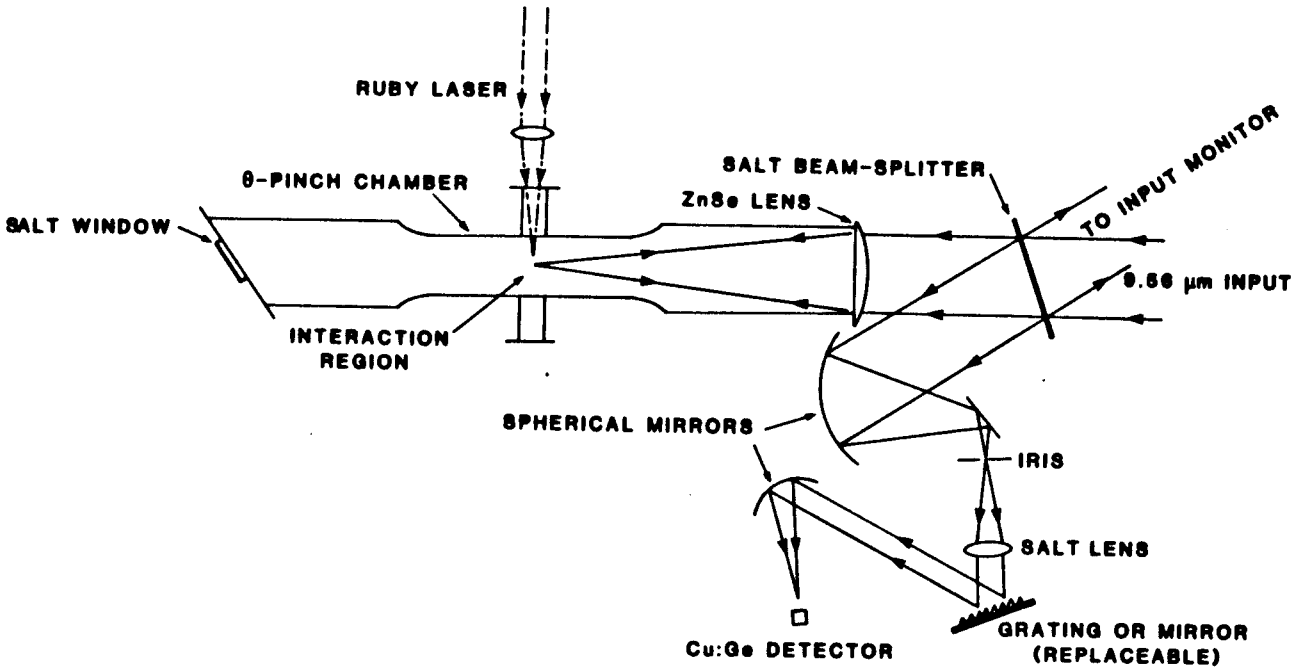
RUBY LASER
θ-PINCH CHAMBER
SALT WINDOW
INTERACTION REGION
SALT BEAM-SPLITTER
ZnSe LENS
TO INPUT MONITOR
9.66 μm INPUT
SPHERICAL MIRRORS
IRIS
SALT LENS
Cu:Ge DETECTOR
GRATING OR MIRROR (REPLACEABLE)

Fig. 21

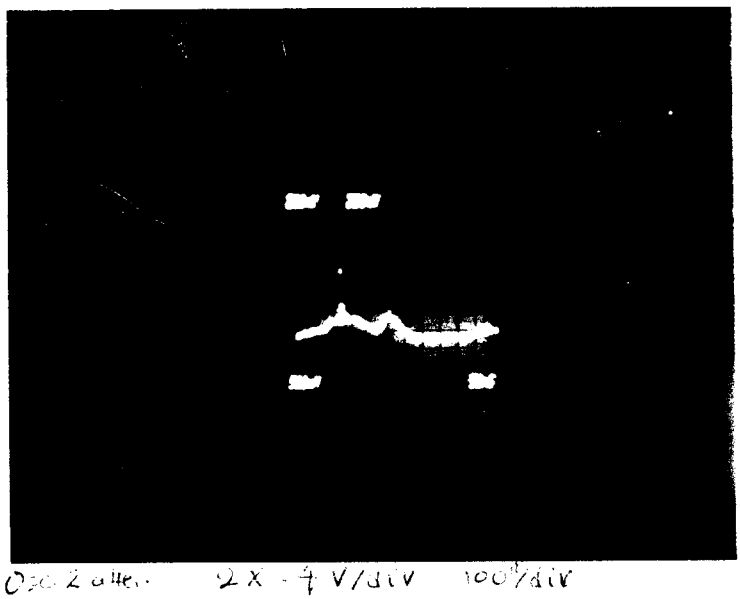

Fig. 22

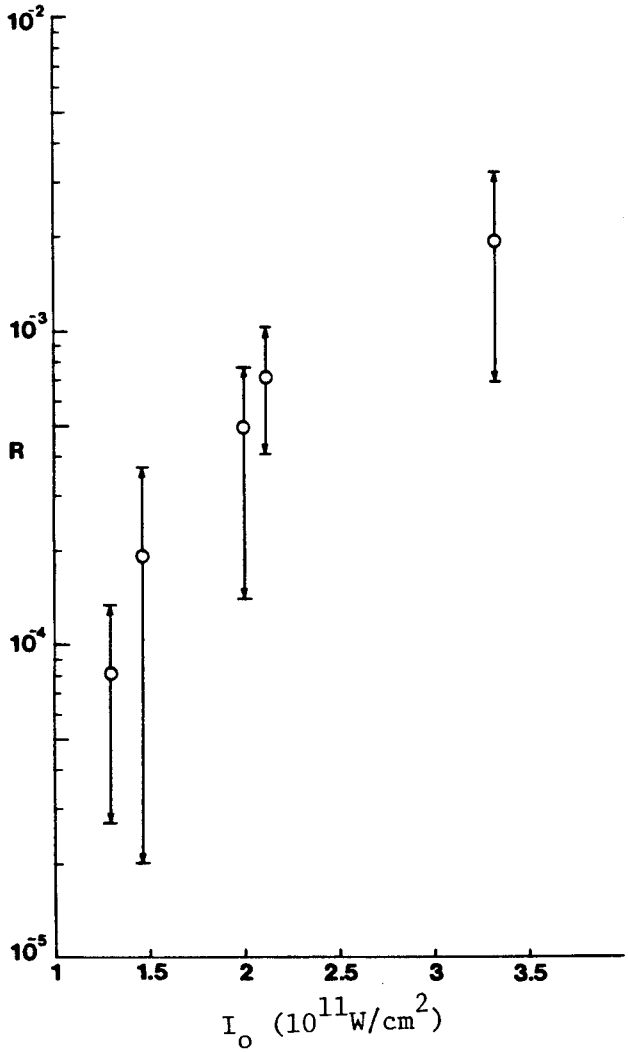
$10^{-2}$
$10^{-3}$
R
$10^{-4}$
$10^{-5}$
1
1.5
2
2.5
3
3.5
$I_o$ ($10^{11}$W/cm$^2$)

Fig. 23

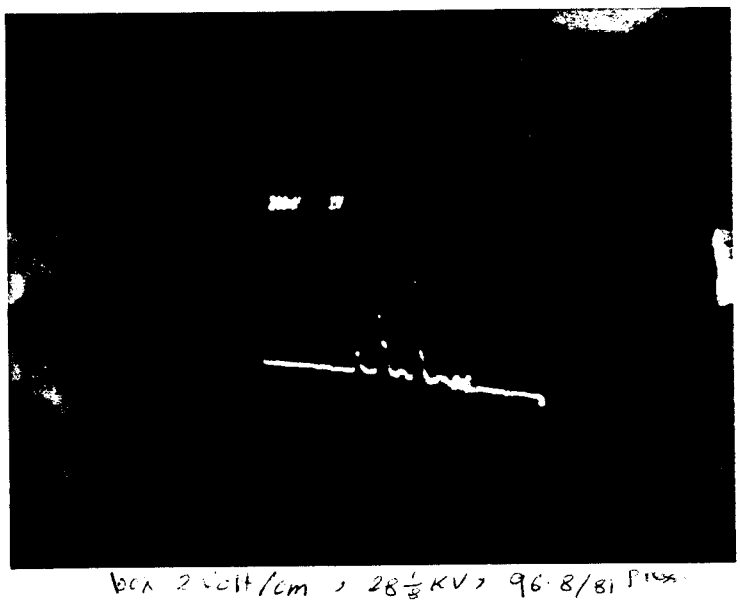
box 2 volt/cm, 28½ KV, 96·8/81 Pics

Fig. 24

In principle, the absolute density from the end-on view can then be adjusted so that the maximum expected radial fringe shift agrees with that in Fig. 14. In this case, an iteration was not necessary because the density calculated from Fig. 13 was $6 \times 10^{16}$ cm$^{-3}$, already sufficiently close to that obtained from Fig. 14.

In Raman scattering, the k-matching condition that determines the inhomogeneous threshold depends mainly on the density, which we can measure well. The temperature is needed only for checking the collisional and Landau damping thresholds. The temperature measurement is difficult, and we have postponed it until now. An estimate can be made from pressure balance, assuming that $\beta = 1$ at maximum compression. At that time, B is not at its maximum, as can be seen from the $\dot{B}$ signal in Fig. 8a. Taking B = 15 kG, we find from $\beta = 1$ that $T_e + T_i \simeq 90$ eV, or $T_e \simeq T_i \simeq 45$ eV if there is thermal equilibrium. (The equilibration time of ≈600 nsec is of the same order as the compression time.) The ion temperature can also be estimated roughly from the compression velocity. It takes 500 nsec to travel 3.5 cm, so the average $v_i$ is ≃ 7 cm/μsec. If we assume that this directed energy is isotropized in the compressed state, setting $\frac{1}{2} Mv_i^2 = \frac{3}{2} KT_i$ yields $T_i \simeq 33$ eV, the same order of magnitude. Thus, the pinch probably produces $T_i \simeq T_e \simeq 40$ eV at $n \simeq 6 \times 10^{16}$ cm$^{-3}$, for an nT product of $2.4 \times 10^{18}$.

In addition, the laser pulse can heat the electrons by inverse bremsstrahlung. For a long cylindrical focal region, radial heat conduction limits $T_e$ to the value (see Appendix B, Eq. 52)

$$T_e = 50\, n_{17}^{2/5}\, P_{10}^{1/5} \text{ eV},$$

where $P_{10}$ is the power (not intensity) in units of $10^{10}$ W. Taking

$n_{17} = 0.6$ and $P_{10} = 0.03$, we obtain $T_e \simeq 20$ eV. Since this is less than what the pinch produces, laser heating has a relatively minor effect on $T_e$ and the ratio $T_e/T_i$. Note that if it were not for radial heat conduction, inverse bremsstrahlung would, in a time t, raise $T_e$ to the value given by

$$T_e^{5/2} - T_{eo}^{5/2} = 3n_{16}I_w t.$$

For t = 30 nsec, $n_{16} = 6$, $Iw = 3 \times 10^{11}$, and $T_{eo} = 40$ eV, this gives $T_e = 125$ eV, or $T_e/T_i \simeq 3$-4. Fortunately, heat conduction prevents such temperature ratios, which would allow SBS to dominate over SRS.

Our plans are to measure $T_i$ and $T_e$ in the immediate future. $T_i$ will be measured by Doppler broadening of He 4686 Å and of impurity lines. $T_e$ will be measured by $90^o$ ruby Thomson scattering. The scattering parameter $\alpha$ under standard conditions is $\alpha \simeq 0.4$. This is not small enough that collective effects can be neglected. $T_e$ cannot be obtained by simply measuring the width of the spectrum; the latter will have to be compared with computed spectra in the intermediate-$\alpha$ regime.

Note that the same Thomson scattering system, set up at $\theta = 7.5^o$, will measure the SRS plasma waves with $k = 2k_o$, just as it was used for SBS ion waves at the same wavelength.

3. Scattering measurements

The experimental set-up for stimulated Raman scattering is shown in Fig. 21. The 9.56-μm input beam is focused with an f/7.2 lens along the axis of the θ-pinch and is dumped through a salt window at the far end. The reflected light is collected by a beam splitter and focused onto a cooled Cu:Ge detector after passing through an infrared spectrometer. In anticipation of beat-frequency experiments, an $SF_6$ cell was introduced into the $CO_2$ oscillator cavity to allow two lines at 9.56 and 10.27 μm to

be produced with variable intensity ratio, as was done previously.[10, 11] Hence, the pump was at 9.56 μm instead of the usual 10.6 μm. The focused intensity was $3.3 \times 10^{11}$ W/cm$^2$ in a 300-μm diam spot and a 50 nsec FWHM pulse. The measured plasma density was $6 \times 10^{16}$ cm$^{-3}$ (in He).

To observe SRS, it was necessary to time the laser pulse so that it comes during a 100-nsec window at the first compression of the θ-pinch, when the density is maximum and is not changing rapidly. At this time, one expects the density to be relatively uniform and the temperature ratio $T_i/T_e$ to be $\geq 1$ so that SBS is suppressed. A typical pulse is shown in Fig. 22, which is a superposition of three signals on one trace. The first broad peak is the photodiode signal used to monitor plasma density. The sharp spike at the peak of this signal is the SRS scattered light. The second broad peak is the input monitor, delayed by 150 nsec so as to be seen on the single-trace storage scope. Because of jitter, not all pulses have sufficiently good timing to produce SRS. A dual-beam storage scope is needed to check the timing before hard data can be obtained. (The scope has been ordered on NSF funds.)

Frequency analysis shows that the scattered light is at 10.47 μm, corresponding to $n = 8 \times 10^{16}$ cm$^{-3}$, in fairly good agreement with the independent measurement of density. By attenuating the pump beam, a preliminary growth curve of Raman reflectivity R vs. $I_o$ has been obtained. This is shown in Fig. 23. We have so far a maximum intensity only two times the threshold value. The individual Raman spikes are about 2 nsec FWHM. An example is shown in Fig. 24, which shows three successive spikes on 10 nsec/cm sweep; the detector and scope risetimes are shorter than 1 nsec.

Under other conditions of density and timing, or with other gases,

the same apparatus can produce large Brillouin scatter. To check for SBS under SRS conditions, we tuned the spectrometer to the SBS frequency near 9.56 μm. No measurable signal was seen, so that the SBS level was at least $10^2$ times lower than SRS. In a separate check, the grating spectrometer was replaced by an interference filter combination which has a $10^{-8}$ rejection ratio for 9.56-μm light while passing 10.5-μm light with ≈50% efficiency. The Raman signal was not greatly changed by the filter, indicating that it was not SBS light scattered into the detector.

We next describe an optical mixing experiment in which a second, lower-frequency beam at $\omega = \omega_2$ was injected in the direction opposite to the 9.56 μm pump at $\omega = \omega_o$. Since optical mixing with laser beams such that $\omega_o - \omega_2 = \omega_p$ was first reported by Stanfield et al.,[(a)] many groups, including ourselves almost 10 years ago, have proposed to do the experiment better with $CO_2$ lasers. Up to now, no one had succeeded. The arrangement is shown in Fig. 25 and is the same as in the SRS experiment except for the 10.27 μm backward beam from the same laser. The frequency difference of the two beams resonates with a plasma density of $6 \times 10^{16}$ $cm^{-3}$. The two beams must coincide in space and time, and both must be timed to arrive when the density has the right value. The path lengths of the two beams are carefully matched, and the 10.27-μm beam is weakly focused to about 6 mm diameter, so that it easily overlaps the 300-μm diam 9.56 μm beam. The intensity ratio is about $10^{-4}$, the "red" beam being only $2 \times 10^7$ $W/cm^2$.

Optical mixing is not a nonlinear parametric instability but is linear in the two intensities. Frequency matching requires $\hbar\omega_o = \hbar\omega_2 + \hbar\omega_p$.

---

(a) B. L. Stanfield, R. Nodwell, and J. Meyer, Phys. Rev. Lett. 26, 1219 (1971).

This can be viewed as the breakup of a quantum of $\omega_o$ light into a quantum of $\omega_2$ light and a plasmon. Thus, the intensity of the higher frequency beam decreases, and that of the lower frequency beam increases. This is the reason the backward "tickler" beam had to have longer wavelength than the pump. It is easier to detect a large fractional increase in the intensity of the red beam than a small decrease in the intensity of the pump.

However, there is a difficulty that did not become apparent until we actually did the experiment. Since the $\omega_o$ beam is more sharply focused than the $\omega_2$ beam, most of the $\omega_2$ light does not pass through the interaction region. The <u>average</u> amplification of the $\omega_2$ beam is miniscule. Furthermore, SRS would produce light at the same $\omega_2$ frequency. The solution is to misalign the two beams slightly and then to block the $\omega_2$ beam after it has been brought to a focus by the ZnSe lens (Fig. 25). The spectrometer and detector are placed 4.5 m away from the lens, so that when they are aligned to receive the unblocked 10.27 μm beam, they do not see most of the backscattered light, which retraces the path of the 9.56 μm beam and is therefore misaligned. When the $\omega_2$ beam is blocked and there is no interaction (wrong plasma density), there is only a low level of stray light. When optical resonance occurs, those rays of $\omega_2$ light which coincide with rays of $\omega_o$ light are amplified. Since the amplified rays diverge from the focus and do not hit the lens as a parallel beam, they are focused by the lens at a different place and miss the beam block. Fig. 26 shows an example of the amplified $\omega_2$ signal; it is usually 25-60 times the stray light level and went way off scale on this shot.

This experiment has not yet progressed to the data-taking stage, but we have made several checks. When the $\omega_2$ beam is not present, there

is no SRS: the $\omega_o$ beam is kept below threshold. When the laser pulse is mistimed so that is comes at a different time in the θ-pinch pulse, the density is wrong and no amplification is seen. In the future it should be possible to detect the plasma wave directly by ruby Thomson scattering at $\theta=7.5^o$. A further check would be to interchange the frequencies of the pump and tickler beams to see that the effect disappears.

C. Theory and Computation

1. Effect of SBS on SRS

Since SBS usually has a lower threshold than SRS, it is difficult to observe SRS without the ion waves from SBS being present in the plasma. These ion waves modulate the density in a quasi-dc fashion, forcing the SRS plasma waves to grow in an inhomogeneous medium. We anticipated two opposing effects. First, the density depressions could trap the plasma waves, causing a convective instability to become absolute. Second, the density ripples could cause the plasma waves to be nonsinusoidal; that is, to develop spatial harmonics with larger k, so that Landau damping would be enhanced. To see which effect would dominate and whether SRS would be enhanced or suppressed by SBS, we made a study with Dr. H. C. Barr, a visiting professor from the University of Wales and Rutherford Laboratory, England.

We first studied the fluid equations for SRS in a density ripple, obtaining he usual Mathieu equation previously considered by Kaw, Lin, and Dawson[(b)]. What is special here is that in an underdense plasma the ripple created by SBS has $k \simeq 2k_o$, almost exactly the same as the k of

---

(b) P. K. Kaw, A. T. Lin, and J. M. Dawson, Phys. Fluids 16, 1967 (1973).

the plasma wave. Furthermore, the ion wave can be so large that the coefficient q of the cosine term in the Mathieu equation cannot be treated with the small-q approximation. Physically, large q means that the thermal term $3k^2v_e^2$ in the Bohm-Gross dispersion relation cannot overcome the change in $\omega_p$, so the plasma waves are trapped in the density troughs. The fluid equations, however, do not contain Landau damping, and the major part of this work was done with a full kinetic treatment. The main effect we found was unexpected. The plasma wave at $k \simeq 2k_o$ couples to the density ripple, also at $k \simeq 2k_o$, to give harmonics at $k \simeq \pm 2nk_o$. The strongest coupling is to the n=0 mode, for which $k \simeq 0$. This gives rise to a strong backward plasma wave at $k \simeq -2k_o$. The modes at $\pm 4nk_o$ have more Landau damping and are less important. The $k = 0$ mode is not Landau damped, and the $k = -2k_o$ mode is a reflection of the plasma wave, enhancing its interaction. It appears that whatever effect SBS has is in a direction to lower the SRS threshold. This work is not yet ready for publication.

2. Computations of electron acceleration

A new student, Warren Mori, has been put to work under the supervision of John Dawson to do one-dimensional simulations of the laser acceleration scheme to be described in Sec. IIIC. Some of his results will be given in that section.

## IV. SCIENTIFIC COLLABORATORS

The work reported here was carried out by the principal investigators, Professor F. F. Chen and Adjunct Associate Professor C. Joshi, in collaboration with two students, Chris Clayton and Behrouz Amini, who completed their dissertations with support from this grant.

The group was fortunate to be joined by Dr. H. C. Barr of the University College of North Wales, Bangor, U.K., who spent part of his sabbatical at UCLA and worked on the theory of Raman scattering in the presence of Brillouin scattering.

In the first year of this period, we similarly benefited from a sabbatical visit by Prof. Akio Yasuda of Tokyo Univeristy of Mercantile Marine, who collaborated in the experimental measurements.

## V. THESIS ABSTRACTS

1. Christopher Clayton

2. Behrouz Amini

ABSTRACT OF THE DISSERTATION

The Physics of the Ion Acoustic Wave
Driven By
the Stimulated Brillouin Scattering Instability

by

Christopher Emmet Clayton
Doctor of Philosophy in Engineering
University of California, Los Angeles, 1984
Professor F. F. Chen, Chair

The ion acoustic wave excited in the stimulated Brillouin scattering (SBS) instability is probed via collective ruby-laser Thomson scattering in order to understand the low saturation level observed in the instability. Many of the features observed in the Brillouin backscattered $CO_2$ laser light from the underdense gas-target plasma are also observed in the Thomson scattered ruby light--from which it is learned that the ion acoustic wave grows exponentially and then saturates as the $CO_2$ pump power is increased. The primary advantage of the ruby Thomson scattering diagnostic is in its capability of providing simutaneous space- and time-resolved measurements of the ion wave amplitude. From these first such detailed measurements, we

find that the ion wave grows exponentially in space at a rate which agrees with the linear convective SBS theory. However, at higher pump powers, the ion wave saturates at an inferred amplitude of $\tilde{n}/n_0 \simeq 5\text{-}10\%$. Further increases in the pump power appear to result in an increase in the length over which the ion wave is saturated. A nearly constant SBS reflectivity in this saturated regime, however, suggests that the saturated ion wave does not contribute as much to the scattered power as would be expected from Bragg scattering theory. This apparent contradiction can be resolved if ion trapping is responsible for the saturation of the ion wave. The saturation amplitude of the ion wave is consistent with estimated thresholds for ion trapping effects to become important. Discrete harmonics of the ion wave are also detected in the spectrum of the ion wave. However, their apparent linear dependence on the amplitude of the fundamental suggest that their presence is not directly related to the observed saturation.

ABSTRACT OF THE DISSERTATION

by

Behrouz Amini

Doctor of Philosophy in Engineering

University of California, Los Angeles, 1984

Professor F. F. Chen, Chair

Experimental results on stimulated Raman backscattering induced by $CO_2$ laser light in a fully ionized plasma will be presented. Stimulated Brillouin scattering, which has always been the dominant process in all other experiments, is totally suppressed here; this is believed to be due to heavy Landau damping of the acoustic wave, in agreement with the estimated ion temperature.

By ruby laser scattering we have measured the initial density fluctuation of plasma waves and, as a result, the number of e-foldings for the scattered wave to reach to the detectable limit. It is only then that one can make a proper comparison between the theory and the experiment. The discrepancies between the theoretical prediction and the experimental results are fully discussed.

We have achieved the excitation of electron plasma waves in a hot, fully ionized and well diagnosed plasma and the detection of the excited

electrostatic waves by light scattering. Two counter-propagating $CO_2$ laser beams are used for the excitation; and a third beam, from a ruby laser, is used for the detection by Thomson scattering.

In the absence of the pump beams, plasma satellites are seen in the Thomson-scattered light; the Bohm-Gross frequency is therefore measured directly. When the pump beam is on, the enhancement of the scattered light by orders of magnitude indicates the strong coupling of the laser with the plasma when the Bohm-Gross frequency matches the difference frequency between the two pumps. Due to this strong coupling, this mechanism can be used (among other applications) as an excellent heating technique for laboratory fusion devices.